Study of Effects of Deformation in Nb_3Sn Multifilamentary Strands

E. Barzi, M. Bossert, V. V. Kashikhin, A. Kikuchi, D. Turrioni, R. Yamada, A. V. Zlobin

***Abstract*— In the process that leads a flawless Nb_3Sn round strand to become part of a Rutherford cable first, and of a coil next, the same cabling process affects strands of different kinds in different ways, from filament shearing to subelement merging to composite decoupling. Due to plastic deformation, after cabling the filament size distributions in a strand usually change. The average filament size typically increases, as does the width of the distribution. This is consistent with the low field transport current of strands in cables being typically lower and less reproducible than for round strands [1]. To better understand the role of filament size in instabilities and to simulate cabling deformations, strands to be used in cables can be tested by rolling them down to decreasing sizes to cover an ample range of relative deformations. A procedure is herein proposed that uses both microscopic analysis and macroscopic measurements of material properties to study the effects of deformation.**

***Index Terms*— Nb_3Sn, Rutherford cable, critical current density, magnetic instability.**

I. Introduction

BOTH success and failure were observed on high field dipole magnet models made at Fermilab. Whereas 10 T was obtained by reaching short sample limits in a racetrack, mirror and three dipoles [2,3] made of Powder-in-Tube (PIT) Nb_3Sn strands, only 50% of the expected performance was achieved by two dipole mirrors [3] made of first generation Restack Rod Process (RRP) strands.

Several factors can degrade the performance of a Nb_3Sn virgin strand. Plastic deformation during cabling, precompression during magnet fabrication, and Lorentz forces during operation are present at high fields. In the low field region, where magnetic instability is prevalent, filament deformation is especially important. In an effort to understand the behavior of different strands during cabling, rolling was chosen as it produces a homogenous deformation along the length of the strand, and presumably also a reproducible number of defects under strain. The strand under study is rolled down to smaller thicknesses to cover a large range of deformations. Rolled strands are then used both for microscopy analysis, and I_c and magnetization measurements.

The analysis procedure starts by identification of the various types of defects observed in a given SC material. At each stage of the deformation, filament size distributions are measured, defects counted, and high and low field SC properties measured. For example this allows comparing strands of various designs. To correlate deformation to that seen in a cable, these same aspects can be obtained for strands in the cable in question.

This procedure was applied first to compare RRP and PIT strand behavior, to study the effect of annealing RRP material before cabling, to measure the effect of increased Cu thickness between subelements in a novel design produced by OST, and finally to verify how much damage is already present before reaction and how much occurs during reaction.

II. Strand Description

A number of multifilamentary RRP and PIT strands by Oxford Superconducting Technology (OST) and ShapeMetal Innovation (SMI) were used for this study. Strand parameters are summarized in Table I, and some strand cross sections are shown in Fig. 1. The 1 mm PIT strand with 192 filaments was used to fabricate all the aforementioned PIT coils. Of the RRP materials, the 108/127 subelement (SE) strand RRP1 of 1 mm size was used to fabricate a single layer small racetrack which performed at 100% of short sample limit [4] and a shell-type half-dipole to be tested in a mirror configuration. The early 54/61 filament strand RRP4 of 0.7 mm size was used to fabricate the two dipole mirrors that did not perform well. The RRP2 strand is a 60/61 SE strand with increased Cu spacing between SE's, and RRP3 is the latest generation of the original 54/61 SE design [1].

TABLE I
Strands Description

Strand ID	PIT	RRP1	RRP2	RRP3	RRP4
Billet ID	187	8195-97	8853	8817	7054-60
No. of filaments	192	108/127	60/61	54/61	54/61
Strand diameter, mm	1.0	1.0	0.7	0.7	0.7
I_c(12 T), A	~700	~900	>550	530-560	420-520
D_{eff}, μm	45	84	-	79	85
Geometric filament size, μm	50-57	64-75	57-71	59-74	61-75
RRR	250	300	200	200	40
Twist pitch, mm	20	12	12	13.5	12
Cu fr., %	52	49	46	46.5	50

Manuscript received August 28, 2006. This work was supported by the U.S. Department of Energy.

All Authors but Akihiro Kikuchi are with Fermi National Accelerator Laboratory, Batavia, IL 60510 USA (D. Turrioni phone: 630-840-3695; fax: 630-840-3369; e-mail: turrioni@fnal.gov).

Kikuchi is with NIMS, Tsukuba, Japan.

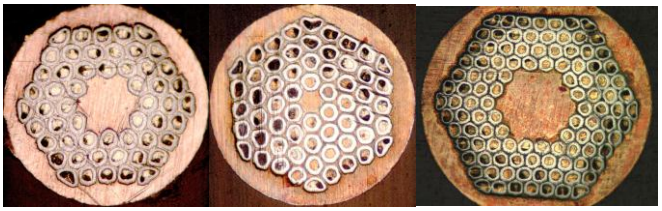

Fig. 1. RRP3 strand with 54/61 SE's (left), RRP2 strand with 60/61 spaced SE's (center), and RRP1 strand with 108/127 SE's (right).

III. Sample Preparation and Test Procedures

The strand samples were wound and heat treated in Argon atmosphere according to schedules that were appropriate to each strand on grooved cylindrical barrels made of Ti-alloy (Ti-6Al-4V). After reaction, the samples were tested on the same barrel. The I_c was determined from the voltage-current (V-I) curve using the 10^{-14} Ω·m resistivity criterion. Magnetization was measured using a balanced coil magnetometer with a magnetic field ramp rate of 17 mT/s.

Two orientations with respect to the external magnetic field were used to test the rolled strand samples. These are the short edge configuration, where the longest size of the strand is perpendicular to the field, and the long edge configuration, where it is the shortest size of the strand that is perpendicular to the field. The I_c was measured in both configurations, magnetization on the long edge only.

The geometric filament sizes were obtained using a high-resolution optical microscope equipped with an imaging software that allows measuring lengths with pixel resolution, i.e. 0.72 μm. The short and long diameters were measured for all filaments (as in Fig. 2) on a number of cross sections with a precision of ±1 μm. The estimated accuracy was $^{+0\%}_{-2.5\%}$.

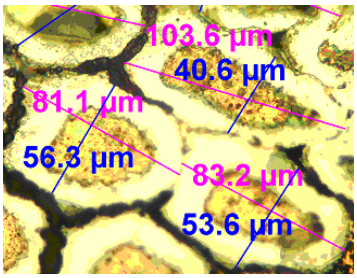

Fig. 2. Example of measurement of long and short diameters of Nb_3Sn subelements.

IV. Microscopic Analysis

A. Damage Analysis

Five mutually exclusive sub-categories of defects were found so far in this analysis of deformed Nb_3Sn strands. They are pictured as A to E in Fig. 3. Defects of each kind of these five identified sub-categories were counted on several cross sections of rolled strands at each stage of the deformation. Defects A, B and D were subsequently assembled into the "broken SE" category, defects B to E into the "merged SE" category. The number of merged and/or broken SE's can be plotted as a function of relative strand deformation (see for instance Figs. 9, 10). Adequate statistics have to be determined to tailor uncertainty to the accuracy needed by the phenomenon under study.

B. Filament Size Distributions

A number of cross sections of rolled strands were analyzed at each stage of the deformation. The short and long diameters can be measured for all SE's to obtain size distributions.

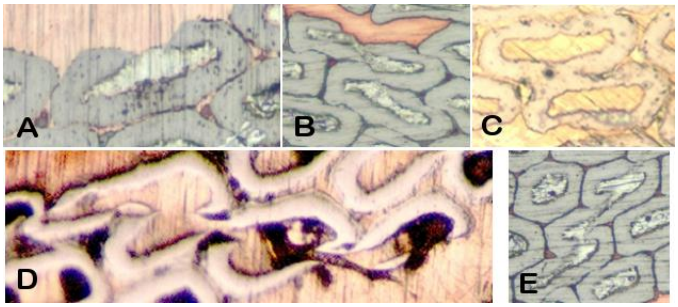

Fig. 3. Defects found in modern Nb_3Sn strands: A) broken only, B) broken and Nb merged, C) Nb merged, D) broken and Sn merged, E) Sn merged.

V. Superconducting Properties

A. Critical Current and Residual Resistivity Ratio (RRR)

The rolled strand's I_c in the high field range as a function of deformation is a measure of its sensitivity to strain. However, results on rolled strands are not conclusive before comparing them with the performance of cables or extracted strands, since the cabling process can produce localized stress concentrations that are absent in an homogeneous rolling procedure. The same can be said of RRR, which in rolling degrades homogenously in the strand due to uniform barrier thinning.

B. Magnetization

Contrary to cabled strands, where the merging between SE's is a local effect, in rolling the deformation is continuous along the length of the strand. This produces a measurable and reproducible number of merged SE's as a function of deformation. In this case, merging can be observed through magnetization measurements too.

VI. Results and Discussion

A. Comparison between RRP and PIT

It was found that RRP and PIT strands behave very differently. Despite filament relative deformation being very similar for the two (shown in Fig. 4 for 1 mm strands RRP1 and PIT), at increasing deformations RRP strands manifest some breaking, but also increasing merging between SE's, whereas PIT tubes show only some breaking under shearing. This is apparent from the plots in Fig. 5, which shows the number of broken and merged filaments as a function of relative deformation for both strands. Relative deformation is defined as $(\text{diameter}_{\text{initial}} - \text{diameter}_{\text{final}})/\ \text{diameter}_{\text{initial}}$. This difference in behavior can be observed also with

magnetization. Whereas in PIT the magnetization of increasingly thinner strands decrease as expected consistently with a negligible merging, in RRP1 the magnetization amplitude decrease down to 20% deformation, but starts increasing in a random manner above this threshold, as evidenced by the plots in Fig. 6. The randomness is due to the random orientation with respect to the field with which SE merging occurs.

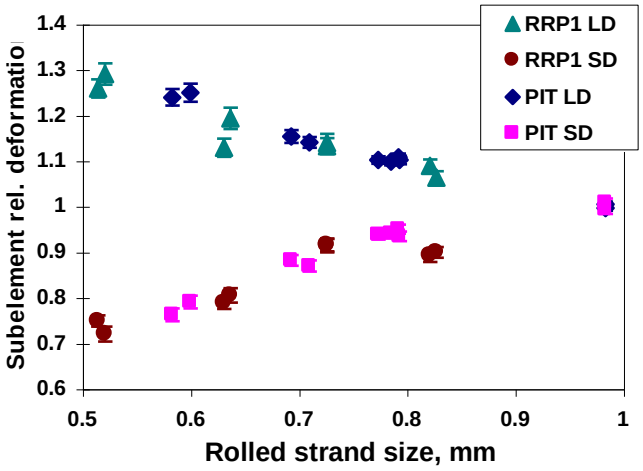

Fig. 4. Relative long and short diameter deformation for RRP1 and PIT rolled strands as a function of rolled strand size.

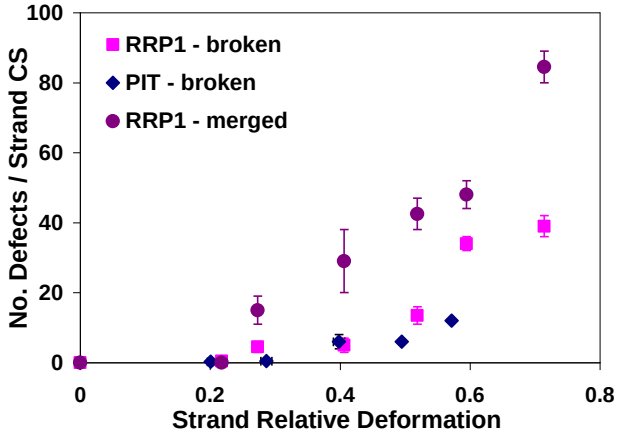

Fig. 5. Average number of defects per strand cross section as a function of strand relative deformation for RRP1 and PIT.

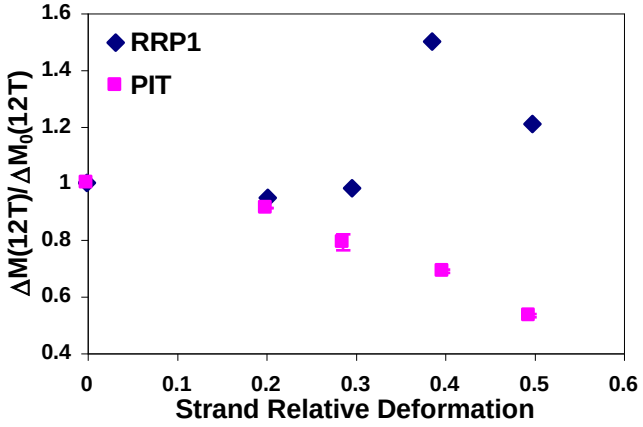

Fig. 6. Average magnetization amplitude at 12 T normalized to that of the round strand as a function of strand relative deformation for RRP1 and PIT.

The average I_c(12 T) of the rolled strand normalized to that of the round wire as a function of strand relative deformation is given for RRP1 and PIT in Fig. 7. To determine which rolling deformation best represents the strand in a cable, the I_c results of its extracted strands have to be compared to those of the rolled strands. This has to be done at least once for a given strand design, as different strand designs can behave quite differently. It was found that I_c degradation due to cabling is more sensitive to strand design than to cable geometry [5]. The average RRR of the rolled strand normalized to that of the round wire as a function of strand relative deformation (Fig. 8) was found to be very similar for RRP1 and PIT. This is consistent with the well known dependence of RRR vs. Cu cold work.

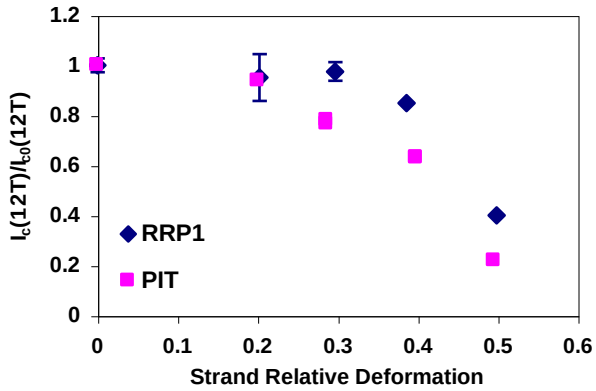

Fig. 7. Average I_c(12 T) of the rolled strand normalized to that of the round wire as a function of strand relative deformation for RRP1 and PIT.

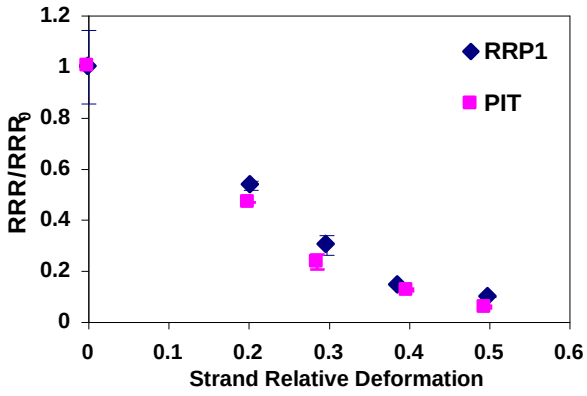

Fig. 8. Average RRR of the rolled strand normalized to that of the round wire as a function of strand relative deformation for RRP1 and PIT.

B. Effect of Annealing

In an attempt to reduce strand deformation and damage during cabling, an experiment was performed on non-annealed and annealed RRP round and increasingly deformed strands. The microscopic analysis did not show any appreciable differences in the number of broken and merged filaments.

C. Effect of Increased Subelement Spacing in RRP

To reduce cabling impact on subelement (SE) merging, OST produced a new R&D billet with a Cu thickness between SE's that was increased by about 50% with respect to the standard design. Damage analysis comparisons between the new billet

RRP2 and the latest billet generation of the original design RRP3 are shown in Figs. 9 and 10. The behavior of the first generation standard billet RRP4, which was used in the two FNAL mirrors, is also shown. One can see that whereas SE breakage is comparable among the three billets, their merging behavior is noticeably different. RRP3 has made progress with respect to RRP4, and in the new R&D billet RRP2 merging is at its lowest.

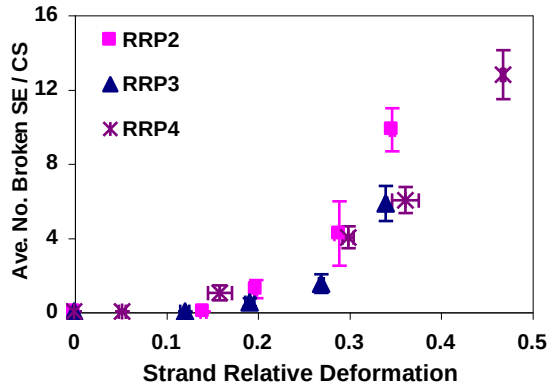

Fig. 9. Average number of broken SE's per strand cross section as a function of strand relative deformation for RRP2 compared with RRP3 and RRP4.

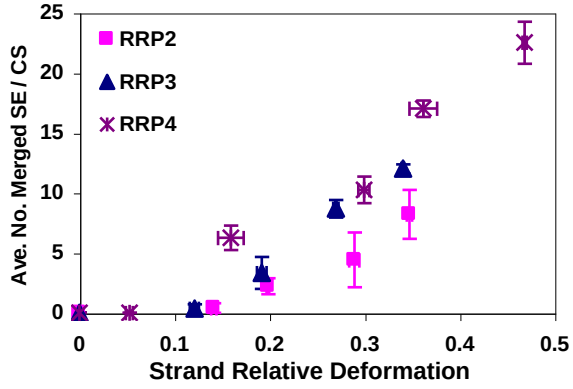

Fig. 10. Average number of merged SE's per strand cross section as a function of strand relative deformation for RRP2 compared with RRP3 and RRP4.

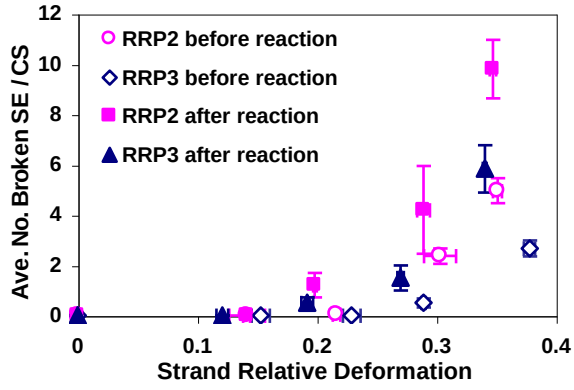

Fig. 11. Average number of broken SE's per strand cross section as a function of strand relative deformation before and after reaction for RRP2 and RRP3.

D. Effect of Reaction

To determine how much damage is caused by deformation before reaction, and what are the effects of heat treating a deformed composite, both RRP2 and RRP3 were used. In both cases, one can see that breakage increases during reaction (Fig. 11). However, whereas in the case of the standard design (RRP3), merging increases noticeably, for the R&D design with increased Cu thickness (RRP2), the merging seen after reaction is on the same level as that obtained in the plastic deformation (Fig. 12). Furthermore, the level of merging before reaction is similar in RRP2 and RRP3. This means that the extra Cu thickness plays its role of providing a barrier to merging not as much during the deformation process as during reaction.

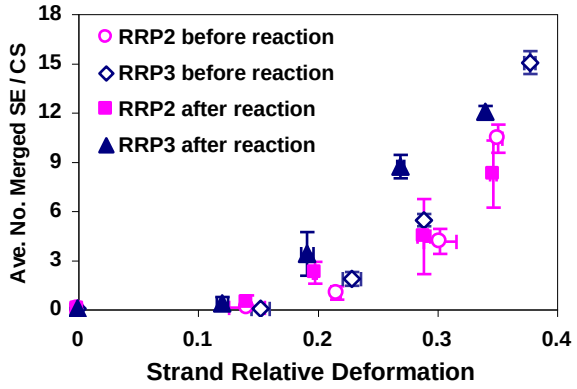

Fig. 12. Average number of merged SE's per strand cross section as a function of strand relative deformation before and after reaction for RRP2 and RRP3.

VII. Conclusion

A procedure that makes use of both microscopic analysis and macroscopic measurements was established to study effects of deformation in brittle superconducting strands. Using this procedure, it was found that in RRP strands, contrary to the PIT case, subelements sometimes merge into each other, creating larger filaments with a somewhat continuous barrier. If filaments are fused together, the strand sees a larger d_{eff} and its instability can dramatically increase locally. Annealing did not show any appreciable improvement in this phenomenon.

Instead, a novel design produced by OST with increased thickness between subelements proved to be effective in reducing merging. It was found that the mechanism by which the extra Cu thickness in the new OST design is effective is that of providing a barrier to merging not as much during the deformation process as during reaction since the level of merging present after deformation is similar in the new and standard strands. The next R&D step is that of implementing the same concept to billets with larger number of restacks.

References

[1] E. Barzi et al., "RRP Strand Studies for LARP", paper 1MK07, this conference.

[2] A.V. Zlobin etal., ""Development and Test of Nb_3Sn Cos-theta Dipoles Based on PIT Strands", IEEE Trans. Appl. Sup., V. 15, No. 2, p. 1160.

[3] S. Feher, "Development and Test of Nb_3Sn Cos-theta Magnets Based on RRP and PIT Strands", IEEE Trans. Appl. Sup., V. 16, No. 2, p. 315.

[4] E. Barzi et al., “Performance of Nb_3Sn RRP Strands and Cables based on a 108/127 Stack Design”, paper 4MW06, this conference.
[5] N. Andreev et al., “Development of Rutherford-type Cables for High Field Accelerator Magnets at Fermilab", paper 1LK07, this conference.